Higd1a is a positive regulator of cytochrome *c* oxidase

Takaharu Hayashi[a,b], Yoshihiro Asano[a,b,1], Yasunori Shintani[a], Hiroshi Aoyama[c], Hidetaka Kioka[b], Osamu Tsukamoto[a], Masahide Hikita[d], Kyoko Shinzawa-Itoh[d], Kazuaki Takafuji[e], Shuichiro Higo[a,b], Hisakazu Kato[a], Satoru Yamazaki[f], Ken Matsuoka[b], Atsushi Nakano[g], Hiroshi Asanuma[h], Masanori Asakura[g], Tetsuo Minamino[b], Yu-ichi Goto[i], Takashi Ogura[d], Masafumi Kitakaze[g], Issei Komuro[j], Yasushi Sakata[b], Tomitake Tsukihara[d,k], Shinya Yoshikawa[d], and Seiji Takashima[a,k,1]

Departments of [a]Medical Biochemistry and [b]Cardiovascular Medicine, [e]Center for Research Education, and [c]Graduate School of Pharmaceutical Science, Osaka University Graduate School of Medicine, Suita, Osaka 565-0871, Japan; [d]Department of Life Science, University of Hyogo, 3-2-1 Kouto, Kamigohri, Akoh, Hyogo 678-1297, Japan; [k]Core Research for Evolutional Science and Technology (CREST), Japan Science and Technology Agency, Kawaguchi, Saitama 332-0012, Japan; Departments of [f]Cell Biology and [g]Clinical Research and Development, National Cerebral and Cardiovascular Center Research Institute, Suita, Osaka 565-8565, Japan; [h]Department of Cardiovascular Science and Technology, Kyoto Prefectural University School of Medicine, Kamigyo-ku, Kyoto 602-8566, Japan; [i]Department of Child Neurology, National Center Hospital of Neurology and Psychiatry, National Center of Neurology and Psychiatry, Kodaira, Tokyo 187-8502, Japan; and [j]Department of Cardiovascular Medicine, Graduate School of Medicine, University of Tokyo, Tokyo 113-8656, Japan

Edited by Gottfried Schatz, University of Basel, Reinach, Switzerland, and approved December 16, 2014 (received for review October 15, 2014)

Cytochrome *c* oxidase (CcO) is the only enzyme that uses oxygen to produce a proton gradient for ATP production during mitochondrial oxidative phosphorylation. Although CcO activity increases in response to hypoxia, the underlying regulatory mechanism remains elusive. By screening for hypoxia-inducible genes in cardiomyocytes, we identified *hypoxia inducible domain family, member 1A* (*Higd1a*) as a positive regulator of CcO. Recombinant Higd1a directly integrated into highly purified CcO and increased its activity. Resonance Raman analysis revealed that Higd1a caused structural changes around heme *a*, the active center that drives the proton pump. Using a mitochondria-targeted ATP biosensor, we showed that knockdown of endogenous Higd1a reduced oxygen consumption and subsequent mitochondrial ATP synthesis, leading to increased cell death in response to hypoxia; all of these phenotypes were rescued by exogenous Higd1a. These results suggest that Higd1a is a previously unidentified regulatory component of CcO, and represents a therapeutic target for diseases associated with reduced CcO activity.

cytochrome *c* oxidase | oxidative phosphorylation | resonance Raman spectroscopy | ATP | oxygen

Cytochrome *c* oxidase (CcO) (ferrocytochrome c: oxygen oxidoreductase, EC 1. 9. 3. 1) is the terminal component of the mitochondrial electron transfer system. CcO couples the oxygen-reducing reaction with the process of proton pumping. Aerobic organisms use this reaction to form a proton gradient across the mitochondrial inner membrane, which is ultimately used by the F_oF_1-ATP synthase to produce ATP.

Mammalian CcO is composed of 13 different subunits (1) containing four redox-active metal centers, two copper sites, and two heme *a* groups. These active centers accept electrons from cytochrome *c* and sequentially donate them to dioxygen. Our group and others have extensively analyzed the link between the oxygen reduction process and proton pumping at the active centers using crystallography, resonance Raman spectroscopy, and Fourier transform infrared spectroscopy (2–4). The metal ions in the copper sites and heme groups in the active centers are individually coordinated by the surrounding amino acids. We have shown that changes in the redox state cause 3D structural changes around the active centers, which in turn leads to alteration of the proton pump mediated by specific amino acid chains that coordinate each metal group (5). Thus, binding of an allosteric regulator close to the active centers might change the efficiency of both electron transfer to oxygen and proton pumping.

Several proteins involved in oxygen supply or metabolism are transcriptionally regulated by intracellular oxygen concentration: vascular endothelial growth factor (VEGF) (6), erythropoietin (EPO) (7), and G0/G1 switch gene 2 (G0s2) for F_oF_1-ATP synthase, as we recently revealed (8). Because CcO is the only enzyme in the body that can use oxygen for energy transduction, it has been suggested that the regulatory mechanism of CcO is dependent on oxygen concentration (9–12); however, this has yet to be demonstrated. In this study, we aimed to identify a regulator of CcO driven by low oxygen concentration.

In this study, by screening for hypoxia-inducible genes, we discovered that *hypoxia inducible domain family, member 1A (Higd1a)* is a positive regulator of CcO. Furthermore, using our recently established ATP-sensitive fluorescence resonance energy transfer (FRET) probe, we demonstrated that Higd1a increased mitochondrial ATP production. We also showed that Higd1a directly bound CcO and changed the structure of its active center.

Results

***Higd1a* Expression Is Induced Early in the Response to Hypoxia.** During the first few hours of hypoxia, CcO and oxidative phosphorylation (OXPHOS) activity is activated, presumably to fully use any remaining oxygen (12). At later time points, metabolism shifts toward glycolysis. Therefore, we hypothesized that a positive regulator of CcO must be up-regulated during an early stage of hypoxia, but down-regulated when glycolysis-related genes become elevated. To identify early hypoxia responsive genes that

Significance

We identified hypoxia-inducible domain family, member 1A (Higd1a) as a positive regulator of cytochrome *c* oxidase (CcO). CcO, the terminal component of the mitochondrial electron transfer system, reductively converts molecular oxygen to water coupled to pump protons across the inner mitochondrial membrane. Higd1a is transiently induced under hypoxic conditions and increases CcO activity by directly interacting with CcO in the vicinity of its active center. Induction of Higd1a leads to increased oxygen consumption and subsequent mitochondrial ATP synthesis, thereby improving cell viability under hypoxia.

Author contributions: Y.A., Y. Shintani, H. Kioka, T.T., S. Yoshikawa, and S.T. designed research; T.H., Y. Shintani, H. Kioka, O.T., M.H., K.S.-I., K.T., and H. Kato performed research; H. Aoyama, M.H., Y.-i.G., T.O., M.K., I.K., Y. Sakata, T.T., and S. Yoshikawa contributed new reagents/analytic tools; T.H., Y. Shintani, S.H., S. Yamazaki, K.M., A.N., H. Asanuma, M.A., and T.M. analyzed data; and T.H., Y. Shintani, H. Kato, T.O., T.T., S. Yoshikawa, and S.T. wrote the paper.

The authors declare no conflict of interest.

This article is a PNAS Direct Submission.

[1]To whom correspondence may be addressed. Email: takasima@cardiology.med.osaka-u.ac.jp or asano@cardiology.med.osaka-u.ac.jp.

This article contains supporting information online at www.pnas.org/lookup/suppl/doi:10.1073/pnas.1419767112/-/DCSupplemental.

might regulate CcO activity, we analyzed gene-expression profiles of neonatal rat cardiomyocytes, one of the most mitochondria-rich cell types, exposed to hypoxic conditions (1% oxygen for 0, 4, or 12 h). Focusing on the genes whose expression was induced more than two-fold at 4 h relative to the prestimulation stage, but then decreased by 12 h, we identified three genes (Fig. 1*A* and Fig. S1 *A* and *B*). Next, we prioritized genes that were (*i*) well conserved among eukaryotes and (*ii*) listed in MitoCarta (13); only one gene, *Higd1a*, satisfied both criteria. To analyze the endogenous expression levels of Higd1a in rat cardiomyocytes, we raised a specific antibody against Higd1a and confirmed its specificity (Fig. S2 *A* and *B*). In cardiomyocytes exposed to hypoxia, Higd1a protein levels increased gradually from 0 to 12 h and then decreased by 24 h (Fig. 1*B*). Immunofluorescence revealed that both endogenous and exogenous Higd1a localized in the mitochondria (Fig. S2*C*).

Higd1a Directly Integrates into the CcO Macromolecular Complex. Because Rcf1a, the yeast homolog of Higd1a, associates with CcO (9–11), we first tested whether mammalian Higd1a binds to CcO in vivo. Indeed, endogenous binding between Higd1a and CcO in rat cardiomyocytes was confirmed by immunocapture with an anti-Higd1a antibody (Fig. S3*A*) and verified by reciprocal coimmunoprecipitation with an anti-Cox4 antibody (Fig. S3*B*). This in vivo interaction was further validated by blue native PAGE (BN-PAGE) of mitochondrial fractions from rat cardiomyocytes (Fig. S3*C*).

Because preparation of the CcO macromolecular complex, which consists of 13 subunits, is technically demanding, it has remained unclear whether Rcf1a/Higd1a binding to CcO is direct. To address this issue, we performed an in vitro pull-down assay using highly purified bovine CcO (hpCcO), which we prepared by dissolving microcrystals used for X-ray structural analysis (14). Notably, recombinant maltose binding protein-fused bovine Higd1a (MBP-Higd1a) (Fig. S4) directly associated with hpCcO (Fig. 1*C*). Furthermore, to assess macromolecular complex formation, we performed BN-PAGE followed by immunoblotting with an antibody against Higd1a, demonstrating that recombinant Higd1a indeed integrated into hpCcO (Fig. 1*D*). With these results, we conclude that Higd1a directly associates and integrates into the CcO macromolecular complex.

Higd1a Causes Structural Changes in CcO and Influences the Active Center of Heme *a*. To explore the relevance of the interaction between Higd1a and CcO, we investigated whether recombinant Higd1a affects hpCcO enzymatic activity. Strikingly, direct addition of MBP-Higd1a to hpCcO significantly increased CcO activity to twice that of hpCcO alone or hpCcO mixed with MBP (Fig. 2*A*). This significant increase in hpCcO activity stimulated by Higd1a led us to speculate that Higd1a causes a structural change at the active centers of CcO.

Therefore, we next investigated whether Higd1a changes the intensity of the visible part of the absorption spectrum of oxidized CcO. MBP alone, used as a negative control, did not cause a significant change in the absorption spectra (Fig. S5). By contrast, MBP-Higd1a caused significant spectral changes at 413 nm and 432 nm (Fig. 2*B*), wavelengths that reflect conformational changes around the hemes in oxidized CcO (15).

To obtain further structural insights, we performed resonance Raman spectroscopy, a powerful and sensitive method for detecting kinetic structural changes that cannot be assessed by X-ray crystal structural analysis. Fig. 2*C* depicts the resonance Raman spectra of CcO with and without MBP-Higd1a, focusing on the heme structure by using 413 nm excitation. The resonance Raman band at 1,372 cm^{-1} in (a: hpCcO) and (b: hpCcO + Higd1a) is assignable to the ν_4 mode of heme and is indicative of ferric heme. After the addition of recombinant Higd1a, the resonance Raman spectra demonstrated two sets of different peaks (or band shifts) at 1,562/1,592 cm^{-1} (the ν_2 mode; a marker for the spin state of heme) (16) and 1,673/1,644 cm^{-1} (the $\nu_{CH=O}$ mode of the formyl group of heme *a*) (17). Importantly, the frequency shift of the band at 1,592 cm^{-1} to 1,562 cm^{-1} is attributable to partial conversion of heme from a low-spin to a high-spin state. In oxidized CcO, only heme *a* includes low-spin iron; therefore, heme *a*, but not heme a_3, is responsible for the band shift (16). These data suggest that the binding of Hig1a to CcO caused structural changes at heme *a*, the active center of CcO.

Higd1a Positively Regulates CcO Activity and Subsequent Mitochondrial OXPHOS. Next, we investigated whether Higd1a truly regulates CcO activity in vivo. To this end, we assessed biochemical CcO activity in rat cardiomyocytes with modified expression of Higd1a. Notably, we observed a significant decrease in CcO activity in Higd1a knockdown cells. This effect was rescued by overexpression of Higd1a, eliminating the possibility of off-target effects in the RNAi experiment (Fig. 3*A*, *Left*). Moreover, overexpression of Higd1a alone increased the basal CcO activity (Fig. 3*A*, *Right*). These data suggest that Higd1a is an endogenous and positive regulator of CcO.

To assess the effect of Higd1a on cellular respiration, we continuously measured the oxygen consumption rate (OCR) using a XF96 Extracellular Flux Analyzer (Seahorse Bioscience).

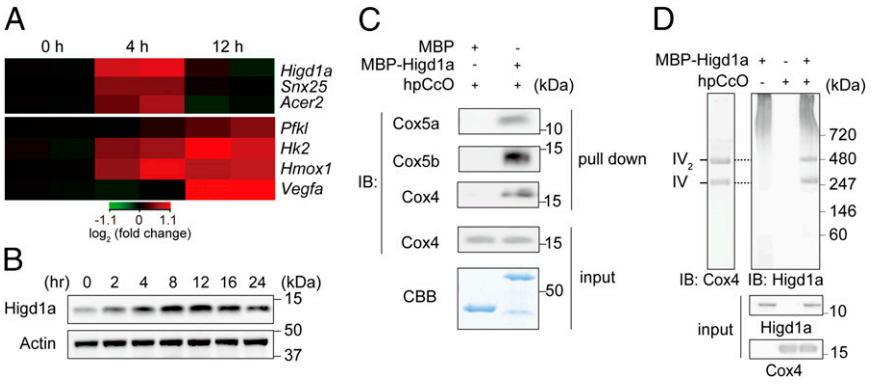

Fig. 1. Hypoxia-inducible Higd1a directly binds to highly purified cytochrome *c* oxidase (hpCcO). (*A*) Heat map of three genes (*Upper*) identified as relatively rapid and transiently induced in response to hypoxia in rat neonatal cardiomyocytes, compared with genes known to be hypoxia inducible (*Pfkl*, *Hk2*, *Hmox1*, and *Vegfa*) (*Lower*). (*B*) Expression of the Higd1a protein was elevated in response to hypoxia. (*C*) In vitro pull-down assay with amylose resin revealed direct binding between MBP-Higd1a and the hpCcO from bovine heart. Loading controls for the hpCcO and MBP-fusion proteins are shown in immunoblots for anti-CcO subunits and CBB staining, respectively. (*D*) MBP-Higd1a directly integrates into hpCcO. Mixed MBP-fusion proteins and hpCcO containing 0.2% *n*-decyl-β-D-maltoside (DM) were resolved by blue native PAGE (BN-PAGE), followed by immunoblotting with anti-Cox4 to detect CcO and anti-Higd1a to detect Higd1a.

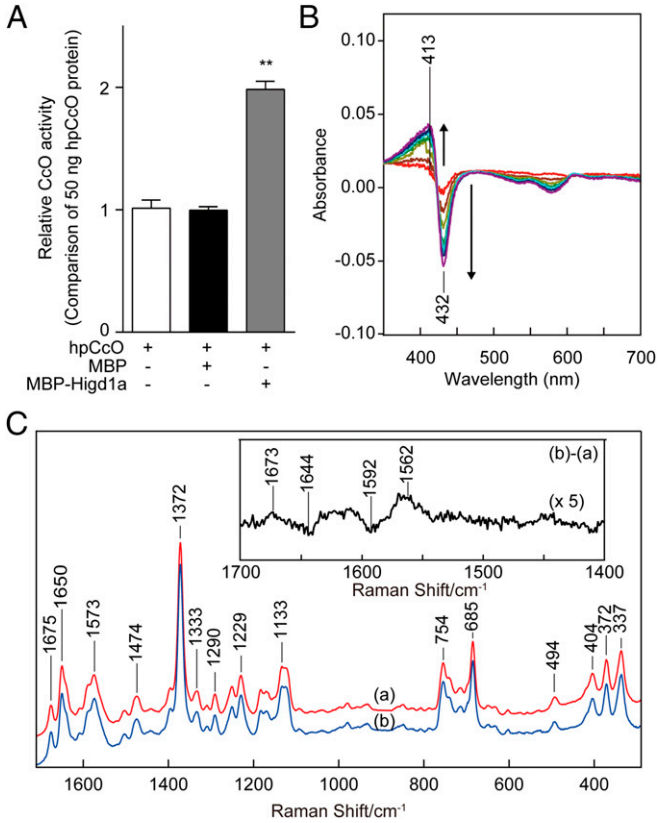

Fig. 2. Higd1a regulates CcO activity through the structural change of the active center in CcO. (*A*) CcO activity of hpCcO and hpCcO with either recombinant MBP or recombinant MBP-Higd1a. MBP-Higd1a causes an increase in CcO activity by almost twofold. Data represent the means ± SEM of five individual experiments. $^{**}P < 0.01$, compared with MBP. (*B*) The difference in absorption spectra between MBP-Higd1a and oxidized hpCcO. MBP-Higd1a caused spectral changes at 413 and 432 nm. Intensity changes of oxidized hpCcO spectra are plotted at 1 min (red), 5 min (brown), 10 min (dark yellow), 15 min (green), 20 min (light blue), 25 min (blue), and 30 min (purple) after adding MPB-Higd1a. (*C*) Resonance Raman spectra of oxidized hpCcO at 0–5 min [spectrum (a)] and oxidized hpCcO mixed with MBP-Higd1a at 0–5 min [spectrum (b)]. The *Inset* shows the difference of the spectra [(b) − (a)].

Knockdown of Higd1a caused a significant decrease in both basal (Fig. S6*A*, *Left*) and maximum OCR, and these effects were rescued by exogenous expression of Higd1a (Fig. 3*B*, *Left*). Moreover, overexpression of Higd1a significantly increased both basal and maximum OCR (Fig. S6*A*, *Right* and Fig. 3*B*, *Right*).

Because the electron transport chain creates a proton gradient that drives F_oF_1-ATP synthase (complex V), ATP production is the overall outcome of mitochondrial OXPHOS. To determine whether modulation of CcO activity by Higd1a affects ATP production, we performed the mitochondrial activity of streptolysin O permeabilized cells (MASC) assay, a sensitive means of measuring the mitochondrial ATP production rate in semi-intact cells (18). Indeed, Higd1a knockdown caused a significant decrease in the ATP production rate relative to the control (Fig. 3*C*), whereas overexpression of Higd1a increased it (Fig. 3*D*). These results suggest that Higd1a modulates mitochondrial OXPHOS through CcO.

Higd1a Protects Cardiomyocytes Under Hypoxic Conditions by Increasing ATP Production. We reasoned that endogenous induction of Higd1a by hypoxia serves to maintain ATP production in mitochondria to the greatest extent possible when oxygen supply is limited. The intramitochondrial matrix ATP concentration ($[ATP]_{mito}$) reflects mitochondrial ATP production far more sensitively than the cytosolic ATP concentration (8). Therefore, we next assessed the effect of Higd1a on ATP production in living cells using the FRET-based mitochondrial ATP biosensor Mit-ATeam (19). First, we examined the effect of KCN, an inhibitor of CcO. KCN significantly reduced the $[ATP]_{mito}$ (Fig. S7), suggesting that Mit-ATeam provides an effective means to monitor the functional consequences of changes in CcO activity. We then confirmed that hypoxia caused a gradual decline in $[ATP]_{mito}$. Overexpression of Higd1a alleviated the decline in $[ATP]_{mito}$ during hypoxia, whereas knockdown of Higd1a accelerated the decrease in $[ATP]_{mito}$ relative to the control (Fig. 4*A*).

The yeast homolog Rcf1 plays a role in respiratory supercomplex stability, and the same is true for Higd2a, but not Higd1a (11). We investigated whether Higd1a affects respiratory supercomplex stability Higd1a-knockdown or -overexpressing cells. As shown in Fig. S8, there was no significant change in the abundance or composition of the respiratory supercomplex, suggesting that the effect of Higd1a described above is not a result of changes in supercomplex stability.

Finally, to test whether the effects of Higd1a on mitochondrial ATP synthesis affected overall cell viability, we analyzed the viability of cardiomyocytes subjected to hypoxia. Under hypoxic conditions, Higd1a-knockdown cells showed a significant increase in cell death, and this effect was rescued by exogenous expression of Higd1a (Fig. 4*B* and Fig. S9*A*). In addition, overexpression of Higd1a alone

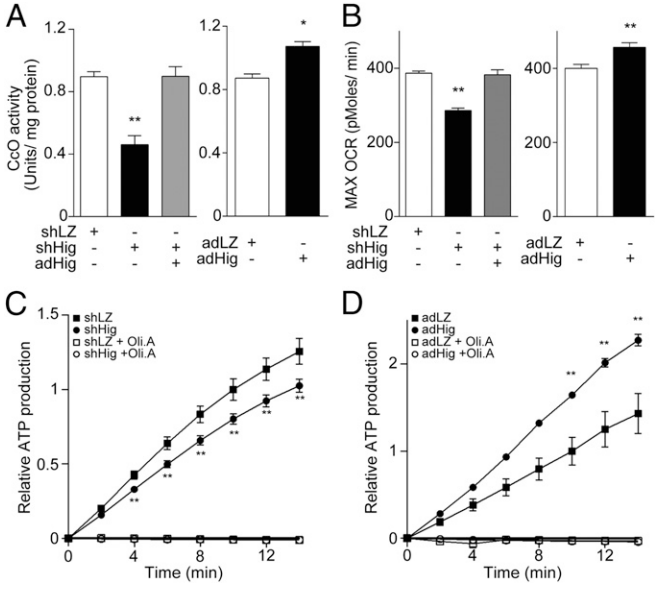

Fig. 3. Higd1a positively modulates mitochondrial respiration by altering CcO activity. (*A*, *Left*) Mitochondrial fraction from rat cardiomyocytes expressing shLacZ (shLZ), shHigd1a (shHig), or both shHig and adHigd1a (adHig) were subjected to the CcO activity assay. (*Right*) CcO activity was measured in cardiomyocytes treated with either adLacZ (adLZ) or adHig. Data represent the means of four individual experiments. (*B*, *Left*) The maximum oxygen consumption rate (max OCR) in rat cardiomyocytes transfected with the indicated adenovirus was measured after treatment with oligomycin A and fluorocarbonyl cyanide phenylhydrazone (FCCP). Knockdown of Higd1a resulted in a significant decrease in max OCR, which was rescued by exogenously expressed Higd1a. (*Right*) Overexpression of Higd1a significantly increased max OCR compared with the cells with adLZ ($n = 20$ for each group). (*C*) The relative ATP production rate of cardiomyocytes treated with shLZ or shHig was measured by the MASC assay ($n = 6$). A numerical value of ATP production at 10 min in shLZ groups is regarded as 1.0. (*D*) The relative ATP production rate of cardiomyocytes treated with adLZ or adHig was measured by MASC assay ($n = 5$). A numerical value of ATP production at 10 min in adLZ groups is regarded as 1.0. Data represent the means ± SEM; $^{*}P < 0.05$, $^{**}P < 0.01$.

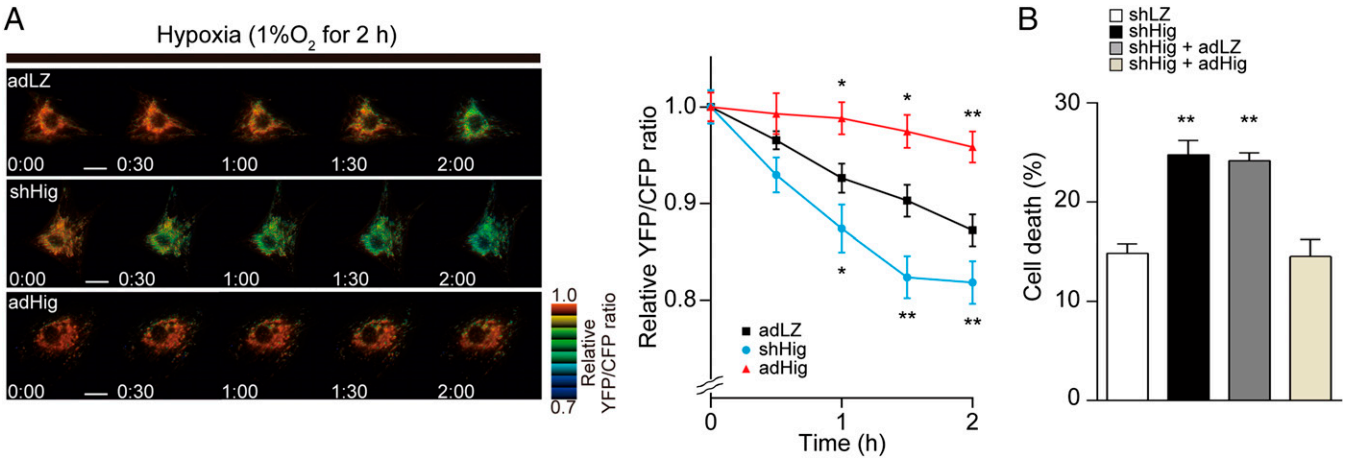

Fig. 4. (*A*) Representative sequential YFP/CFP ratiometric images of Mit-ATeam fluorescence in cardiomyocytes expressing corresponding adenovirus during hypoxia ($n = 12$ for adLZ, $n = 23$ for shHig, $n = 18$ for adHig). All of the measurements were normalized to the ratio at time 0 and compared between adLZ and adHig or shHig. (Scale bar, 20 μm.) (*B*) Cell death of cardiomyocytes treated with shHig was significantly increased compared with the control, which was rescued by addition of adHig under hypoxic conditions for 24 h ($n = 12$ for each group). Data represent the means of three independent cultures, ± SEM; $*P < 0.05$, $**P < 0.01$, compared with control (adLZ or shLZ).

increased cellular tolerance to hypoxia (Fig. S9*B*). On the basis of these findings, we conclude that Higd1a positively regulates CcO activity and subsequently increases mitochondrial ATP production, thereby protecting cardiomyocytes against hypoxia.

Discussion

In this study, we demonstrated that recombinant Higd1a produced in *Escherichia coli* was incorporated into CcO complex purified from bovine heart. The data suggest that Higd1a directly bound to the already assembled CcO complex and increased its activity. Together with the fact that Higd1a expression was rapidly increased by hypoxia, this observation indicated that Higd1a is a positive regulator of CcO that preserves the proton-motive force under hypoxic cellular stress. Physiologically, Higd1a preserved ATP production in healthy cardiomyocytes under hypoxic conditions, which protected them from an energy crisis leading to cell death.

We demonstrated that Higd1a incorporated into the CcO complex and increased its activity. It remains unclear which part of CcO is essential for this change. Higd1a binding may affect the interaction of cytochrome *c* with CcO, modulate internal electron/proton transfer, or modify K_d/K_m for O_2 binding to Cu_B/heme a_3. In fact, the resonance Raman spectroscopy experiment provided us with a clue to this question. First, we discovered that Higd1a markedly shifted the maximum Soret peak around 413 nm absorption, suggesting the occurrence of structural changes in heme that are usually observed during the reduction and oxidation process of CcO. This shift in absorbance prompted us to perform resonance Raman analysis at 413 nm excitation, a powerful tool for investigating the structure of heme and its vicinity. Higd1a induced a frequency shift of the band at 1,592 cm^{-1} to 1,562 cm^{-1} and 1,673/1,644 cm^{-1}; the former frequency is attributed to partial conversion of heme from a low-spin to a high-spin state. In oxidized CcO, only heme *a* includes low-spin iron (16); therefore, heme *a*, but not heme a_3, is responsible for this band shift.

X-ray structural and mutational analyses for bovine heart CcO have demonstrated that protons are pumped through the hydrogen-bond network across the CcO molecule, designated the H pathway, located near heme *a* (20). The driving force for active proton transport is electrostatic repulsion between the proton in the hydrogen-bond network and the net positive charge of heme *a*. One of the critical sites for repulsion is the formyl group of heme *a*, which is hydrogen bonded to Arg38 of the CcO subunit I (21). In our study, resonance Raman spectroscopy revealed specific band shifts from 1,644 cm^{-1} to 1,673 cm^{-1}, which can be attributed to the vibration of the formyl group of heme *a*. This observation suggests that Higd1a binding causes structural changes, particularly around heme *a*, weakening the hydrogen bond between the formyl group and Arg38 of the CcO subunit I, thereby leading to the acceleration of proton pumping efficiency (22). Thus, both band shifts suggest that structural change occurs in the vicinity of heme *a* rather than a_3.

Following the resonance Raman analysis, we sought to determine the Higd1a-CcO binding site via simulation with the COOT software (23), using the previously reported structures of CcO (14) and Higd1a (24). From our structural analysis, CcO contains a cleft composed of relatively few protein subunits near the active centers (Fig. S10*A*). Notably, Higd1a was predicted to integrate into the cleft of CcO near heme *a* and Arg38 (Fig. S10), consistent with the

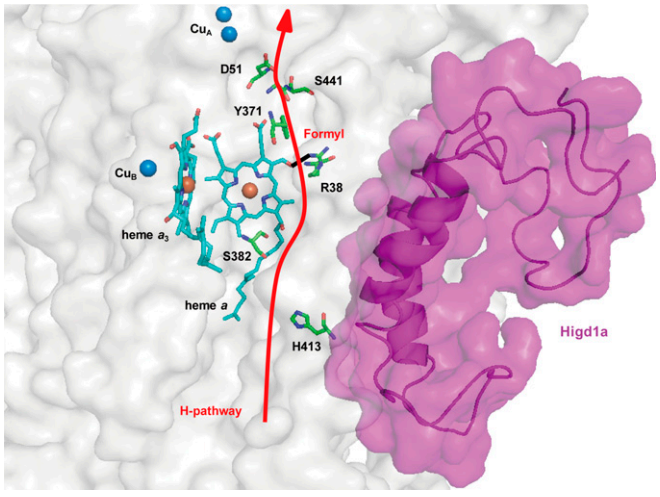

Fig. 5. Higd1a acts on the H pathway. Model depicting our docking simulation (side view) and its relationship with the H pathway. The model shows the location of Higd1a (magenta) in the CcO complex (white) and its relationship to R38 of cytochrome *c* oxidase subunit I and the formyl group of heme *a*, a component of the H pathway (red arrow).

results of the resonance Raman analysis. Thus, it is likely that Higd1a bound to the cleft of CcO, leading to swift structural change around heme *a* and Arg38 and accelerating the proton-pumping H pathway, thereby increasing CcO activity (Fig. 5). Furthermore, when we retrospectively reviewed the purification process of the CcO complex, comprising 13 subunits from the bovine heart, we found that Higd1a remained associated with CcO up to the final step, which required detergent exchange (14). This led us to speculate that Higd1a represents a 14th identified subunit of CcO that is endogenously induced by hypoxia and integrates into the open cleft of CcO to positively regulate its activity. Although the resonance Raman data and docking model simulation are consistent with the idea that Higd1a binding causes structural change around heme *a*, these data are limited because of their speculative nature. Therefore, to confirm these findings, we are currently trying to crystallize the CcO-Higd1a complex to reveal the conformational changes of CcO, particularly around the heme *a* site.

Higd1a was originally identified as a mitochondrial inner membrane protein whose expression is induced by hypoxia (25). Higd1a augments cell survival under hypoxic stress in pancreatic cells (26), and it exerts its protective effect by induction of mitochondrial fission (27). The precise relationship between these reports and our data is not clear. However, our results suggest that the elevation of CcO activity by Higd1a preserves the proton-motive force, which is prerequisite for mitochondria function, thereby leading to increased mitochondrial fission and/or the prevention of apoptosis.

The existence of a direct CcO allosteric activator suggests that there is a structural basis for the intrinsic activation in the CcO complex. To explore this idea further, a screen for small compounds that simply increase the activity of highly purified CcO in vitro has been initiated. Compounds that mimic the effect of Higd1a can preserve ATP production even under hypoxic condition, and hence are expected to exert cellular protective effects particularly when OXPHOS activity is reduced. Recent work showed that lowering the activity of OXPHOS causes the cellular senescence (28), diabetes mellitus (29), and neurodegenerative diseases (30). In addition, several currently intractable mitochondrial diseases are caused by mutations in mitochondrial genes or nuclear genes that lead to dysfunction in mitochondrial OXPHOS. Notably, decreased CcO activity is most frequently observed among patients with mitochondrial diseases (31). Therefore, small compounds that mimic the effect of Higd1a will have therapeutic potential for various acute and chronic diseases including ischemic, metabolic, and mitochondrial diseases.

Materials and Methods

Purification of Recombinant Higd1a Protein. The full-length bovine *Higd1a* cDNA was purchased from GE Healthcare. Then the coding sequence of bovine *Higd1a* was cloned in-frame with an ATG start codon, in the pET21a expression vector (Novagen for overexpression in *E. coli*). A MBP was fused in-frame at the amino terminus for purification. The resulting plasmid was transformed into BL21-Star (DE3; Invitrogen), and the addition of 0.5 mM isopropyl β-D-1-thiogalactopyranoside caused the expression of MBP-Higd1a protein. The cells were sonicated and solubilized by 1% *n*-decyl-β-D-maltoside (DM). The recombinant protein was purified with amylose resin (New England Biolabs), and eluted by 20 mM maltose (pH 6.8 or 8.0, 100 mM sodium phosphate buffer containing 0.2% DM). The eluted protein was concentrated and maltose removed using Amicon Ultra-0.5 10K (Millipore).

Resonance Raman Spectroscopy. Absorption spectra of the samples were measured by a spectrophotometer (Hitachi, U3310) with the path length of 2 mm in 100 mM sodium phosphate buffer (pH 8.0) containing 0.2% DM. The reaction mixture was measured immediately and spectra were recorded every 5 min for 30 min. The protein concentration was 8 μM.

Raman scattering of the samples were measured in a cylindrical spinning cell with excitation at 413.1 nm with a Kr^+ laser (Spectra Physics, model 2060), and the incident power was 500 μW. The detector was a liquid N_2-cooled CCD detector (Roper Scientific, Spec-10: 400B/LN). Raman shifts were calibrated with indene as the frequency standard. Raman spectrum was divided by the "white light" spectrum that was determined by measuring the scattered radiation of an incandescent lamp by a white paper to compensate for the sensitivity difference of each CCD pixel and transmission curve of the notch filter to reject Rayleigh scattering. The accuracy of the peak position of well-defined Raman bands was ±1 cm^{-1}. The protein concentration was 20 μM, and the reaction mixture was incubated for 30 min, before Raman measurements.

Measurement of CcO Activity. CcO activity was measured spectrophotometrically (Shimazu, UV-2450) using a cytochrome *c* oxidase activity kit (Biochain). A total of 25 μg of mitochondrial pellets from cardiomyocytes was lysed with 1% *n*-dodecyl-β-D-maltoside (DDM), and subjected to measurement according to the manufacturer's instructions (32). Concentrations of reduced/oxidized cytochrome *c* were determined using the extinction coefficient at 550 nm of 21.84 $mM^{-1}cm^{-1}$. For in vitro measurement, cytochrome *c* (Sigma) was reduced by ascorbic acid (Wako). Recombinant MBP-Higd1a (20 μM) and hpCcO (20 μM) were incubated at 25 °C for 30 min in the presence of 0.2% DM. After incubation, the mixture and reduced cytochrome *c* were added into the assay buffer, then subjected to measurement at 30 °C (Agilent Technologies, cary300). Slopes of OD_{550} for 1 min were calculated and corrected by a value of hpCcO.

FRET-Based Measurement of Mitochondrial ATP Concentration. FRET-based measurement of mitochondrial ATP concentration in cardiomyocytes was measured as previously described (8, 33). Briefly, FRET signal was measured in cardiomyocytes infected with adenovirus encoding mit-AT1.03 with an Olympus IX-81 inverted fluorescence microscope (Olympus) using a PL APO 60×, 1.35 N.A., oil immersion objective lens (Olympus). Fluorescence emission from Mit-ATeam was imaged by using a dual cooled CCD camera (ORCA-D2; Hamamatsu Photonics) with a dichroic mirror (510 nm) and two emission filters (483/32 nm for CFP and 542/27 nm for YFP; A11400-03; Hamamatsu Photonics). Cells were illuminated using the CoolLED pE-1 excitation system (CoolLED) with a wavelength of 425 nm. Image analysis was performed using MetaMorph (Molecular Devices). The YFP/CFP emission ratio was calculated by dividing pixel by pixel (a YFP image with a CFP image after background subtraction).

Statistical Analyses. The comparison between two groups was made by *t* test (two tailed). For MASC assay, comparison was made by repeated two-way ANOVA. A value of $P < 0.05$ was considered statistically significant. Data represent mean ± SEM.

Further methods are found in *SI Materials and Methods*.

ACKNOWLEDGMENTS. We thank T. Miyazaki (Cyclex) for making antibodies; Y. Okazaki and Y. Tokuzawa (Saitama Medical University) for measurement of CcO activity by cary300; Dr. Steven Coppen for critical reading of the manuscript; S. Ikezawa, E. Takada, and H. Shingu for technical assistance; M. Kobayashi, R. Maki, and the Center for Research Education in Osaka University for MS analysis; Y. Okada for secretarial support; and H. Shimada for discussion and advice. This research was supported by the Japan Society for the Promotion of Science through the "Funding Program for Next Generation World-Leading Researchers (NEXT Program)," initiated by the Council for Science and Technology Policy; grants-in-aid from the Ministry of Health, Labor, and Welfare-Japan; grants-in-aid from the Ministry of Education, Culture, Sports, Science, and Technology-Japan; and grants-in-aid from the Japan Society for the Promotion of Science. This research was also supported by grants from Takeda Science Foundation, Japan Heart Foundation, Japan Cardiovascular Research Foundation, Japan Intractable Diseases Research Foundation, Japan Foundation of Applied Enzymology, Japan Medical Association, Uehara Memorial Foundation, Mochida Memorial Foundation, Banyu Foundation, Naito Foundation, Inoue Foundation for Science, Osaka Medical Research foundation for intractable diseases, Ichiro Kanehara Foundation, and Showa Houkoukai.

1. Tsukihara T, et al. (1996) The whole structure of the 13-subunit oxidized cytochrome c oxidase at 2.8 A. *Science* 272(5265):1136–1144.
2. Morgan JE, Vakkasoglu AS, Lanyi JK, Gennis RB, Maeda A (2010) Coordinating the structural rearrangements associated with unidirectional proton transfer in the bacteriorhodopsin photocycle induced by deprotonation of the proton-release group: A time-resolved difference FTIR spectroscopic study. *Biochemistry* 49(15):3273–3281.
3. Aoyama H, et al. (2009) A peroxide bridge between Fe and Cu ions in the O2 reduction site of fully oxidized cytochrome c oxidase could suppress the proton pump. *Proc Natl Acad Sci USA* 106(7):2165–2169.
4. Ogura T, Kitagawa T (2004) Resonance Raman characterization of the P intermediate in the reaction of bovine cytochrome c oxidase. *Biochim Biophys Acta* 1655(1-3): 290–297.

5. Yoshikawa S, et al. (1998) Redox-coupled crystal structural changes in bovine heart cytochrome c oxidase. *Science* 280(5370):1723–1729.
6. Gospodarowicz D, Abraham JA, Schilling J (1989) Isolation and characterization of a vascular endothelial cell mitogen produced by pituitary-derived folliculo stellate cells. *Proc Natl Acad Sci USA* 86(19):7311–7315.
7. Wang GL, Semenza GL (1993) General involvement of hypoxia-inducible factor 1 in transcriptional response to hypoxia. *Proc Natl Acad Sci USA* 90(9):4304–4308.
8. Kioka H, et al. (2014) Evaluation of intramitochondrial ATP levels identifies G0/G1 switch gene 2 as a positive regulator of oxidative phosphorylation. *Proc Natl Acad Sci USA* 111(1):273–278.
9. Vukotic M, et al. (2012) Rcf1 mediates cytochrome oxidase assembly and respirasome formation, revealing heterogeneity of the enzyme complex. *Cell Metab* 15(3):336–347.
10. Strogolova V, Furness A, Robb-McGrath M, Garlich J, Stuart RA (2012) Rcf1 and Rcf2, members of the hypoxia-induced gene 1 protein family, are critical components of the mitochondrial cytochrome bc1-cytochrome c oxidase supercomplex. *Mol Cell Biol* 32(8):1363–1373.
11. Chen YC, et al. (2012) Identification of a protein mediating respiratory supercomplex stability. *Cell Metab* 15(3):348–360.
12. Fukuda R, et al. (2007) HIF-1 regulates cytochrome oxidase subunits to optimize efficiency of respiration in hypoxic cells. *Cell* 129(1):111–122.
13. Pagliarini DJ, et al. (2008) A mitochondrial protein compendium elucidates complex I disease biology. *Cell* 134(1):112–123.
14. Tsukihara T, et al. (1995) Structures of metal sites of oxidized bovine heart cytochrome c oxidase at 2.8 A. *Science* 269(5227):1069–1074.
15. Wilson DF, Gilmour MV (1967) The low-temperature spectral properties of mammalian cytochrome oxidase. I. The enzyme in intact rat-liver mitochondria. *Biochim Biophys Acta* 143(1):52–61.
16. Heibel GE, Anzenbacher P, Hildebrandt P, Schäfer G (1993) Unusual heme structure in cytochrome aa3 from Sulfolobus acidocaldarius: A resonance Raman investigation. *Biochemistry* 32(40):10878–10884.
17. Babcock GT, Callahan PM (1983) Redox-linked hydrogen bond strength changes in cytochrome a: Implications for a cytochrome oxidase proton pump. *Biochemistry* 22(10):2314–2319.
18. Fujikawa M, Yoshida M (2010) A sensitive, simple assay of mitochondrial ATP synthesis of cultured mammalian cells suitable for high-throughput analysis. *Biochem Biophys Res Commun* 401(4):538–543.
19. Imamura H, et al. (2009) Visualization of ATP levels inside single living cells with fluorescence resonance energy transfer-based genetically encoded indicators. *Proc Natl Acad Sci USA* 106(37):15651–15656.
20. Muramoto K, et al. (2010) Bovine cytochrome c oxidase structures enable O2 reduction with minimization of reactive oxygens and provide a proton-pumping gate. *Proc Natl Acad Sci USA* 107(17):7740–7745.
21. Yoshikawa S, Tsukihara T, Shinzawa-Itoh K (1996) [Crystal structure of fully oxidized cytochrome c-oxidase from the bovine heart at 2.8 A resolution]. *Biokhimiia* 61(11): 1931–1940.
22. Tsukihara T, et al. (2003) The low-spin heme of cytochrome c oxidase as the driving element of the proton-pumping process. *Proc Natl Acad Sci USA* 100(26):15304–15309.
23. Emsley P, Lohkamp B, Scott WG, Cowtan K (2010) Features and development of Coot. *Acta Crystallogr D Biol Crystallogr* 66(Pt 4):486–501.
24. Klammt C, et al. (2012) Facile backbone structure determination of human membrane proteins by NMR spectroscopy. *Nat Methods* 9(8):834–839.
25. Denko N, et al. (2000) Epigenetic regulation of gene expression in cervical cancer cells by the tumor microenvironment. *Clin Cancer Res* 6(2):480–487.
26. Wang J, et al. (2006) Pancreatic beta cells lack a low glucose and O2-inducible mitochondrial protein that augments cell survival. *Proc Natl Acad Sci USA* 103(28): 10636–10641.
27. An HJ, et al. (2013) Higd-1a interacts with Opa1 and is required for the morphological and functional integrity of mitochondria. *Proc Natl Acad Sci USA* 110(32):13014–13019.
28. Horan MP, Pichaud N, Ballard JW (2012) Review: Quantifying mitochondrial dysfunction in complex diseases of aging. *J Gerontol A Biol Sci Med Sci* 67(10): 1022–1035.
29. Saxena R, et al. (2006) Comprehensive association testing of common mitochondrial DNA variation in metabolic disease. *Am J Hum Genet* 79(1):54–61.
30. Lin MT, Beal MF (2006) Mitochondrial dysfunction and oxidative stress in neurodegenerative diseases. *Nature* 443(7113):787–795.
31. Diaz F (2010) Cytochrome c oxidase deficiency: Patients and animal models. *Biochim Biophys Acta* 1802(1):100–110.
32. Berry EA, Trumpower BL (1987) Simultaneous determination of hemes a, b, and c from pyridine hemochrome spectra. *Anal Biochem* 161(1):1–15.
33. Shintani Y, et al. (2014) Toll-like receptor 9 protects non-immune cells from stress by modulating mitochondrial ATP synthesis through the inhibition of SERCA2. *EMBO Rep* 15(4):438–445.

Supporting Information

Hayashi et al. 10.1073/pnas.1419767112

SI Materials and Methods

Antibodies. Antibodies were purchased as follows: Cox4 (Abcam; ab14744), Cox5a (Abcam; ab110262), Cox5b (Abcam; ab110263), Cor1 (Abcam; ab110252), actin (Santa Cruz; sc-1615), HIGD1A (Proteintech; 21749-1-AP), Flag (Sigma; F1804), Vdac (Abcam; ab14734), and Alexa 488- and Alexa 568-labeled secondary antibodies (Invitrogen; A-11001, A-11034, and A-11004). Polyclonal antibodies against Higd1a were generated by immunization with a peptide corresponding to rat Higd1a amino acid sequence (amino acids 2–18, STNTDLSLSSYDEGQGSC) in rabbit.

Cell Culture. Cardiomyocytes obtained from 1-or 2-d-old Wister rats were prepared and cultured in DMEM (Invitrogen) containing 10% (vol/vol) FBS and 100 units/mL penicillin-streptomycin-glutamine. Cells were cultured under 5% CO_2 at 37 °C. For hypoxic exposure, cells were placed in a MCO-5M multigas incubator (Sanyo).

Microarray Data Analysis. Data analysis and normalization were previously mentioned (1). In brief, data analysis was performed using the GeneSpring GX 12.5 bioinformatics software (Agilent Technologies), using the latest gene annotations available. One-way ANOVA test was applied to the filtered gene list, resulting in a group of genes with significant differences. A hierarchical clustering method (heat map constructions) was used to group genes on the basis of similar expression patterns over all samples. Comparisons of the lists of up-regulated genes among them were performed by Venn diagrams.

Constructs. The coding sequence of rat *Higd1a* (NM_080902.3) was amplified by PCR from neonatal rat heart cDNA and cloned into pENTR/D-TOPO (Invitrogen). Next, carboxyl terminus Flag tag was fused by PCR. For adenoviral construction, we used the ViraPower Adenoviral Expression system (Invitrogen) and the BLOCK-iT Adenoviral RNAi Expression system for shRNA (Invitrogen). For shRNA construction, shRNA oligonucleotides were designed as synthetic duplexes with overhanging ends identical to those created by restriction enzyme digestion site. Each oligonucleotide containing a target sequence was subcloned into pENTR-U6 and recombined into pAd/BLOCK-iT-DEST. The target of shRNA for *Higd1a* is the 5′-UTR. The sequences used are as follows: shRNA for *Higd1a*, ccgaagactcttcaagaaa and shRNA for *LacZ*, ctacacaaatcagcgattt. The adenoviral particles were produced by transfection in 293A cells.

Immunoprecipitation. Cardiomyocytes were collected in isotonic buffer (pH 7.4, 25 mM Hepes, 250 mM sucrose, 1 mM EDTA) and mitochondrial pellets were isolated from cell cultures as described (2) with slight modification. Mitochondrial pellets were lysed with lysis buffer (pH 7.4, 30 mM Mops, 150 mM NaCl, 1 mM EDTA, 5% (vol/vol) glycerol containing 1% *n*-dodecyl-β-D-maltoside (DDM)) for 30 min at 4 °C. After a clarifying spin, samples were incubated with individual antibodies for 2 h at 4 °C followed by addition of protein G Sepharose (GE Healthcare) for 30 min at 4 °C. After washing, the bound proteins were eluted with SDS/PAGE sample buffer.

Immunoblotting. The 200×10^4 cardiomyocytes treated under 1% oxygen were lysed in pH 7.4, 30 mM Mops, 150 mM NaCl, 1 mM EDTA, 5% (vol/vol) glycerol, 1% DDM, protease inhibitor mixtures (Amresco). After centrifugation for 5 min at $21{,}900 \times g$ to remove insoluble material, lysates were assessed for protein levels using the BCA method (Pierce) and 4 μg of soluble protein from each was resolved on 12% Bis-Tris gels 160 V for 45 min. Gels were transferred to PVDF and Western blotted.

Immunofluorescence Assay. Cardiomyocytes were seeded on collagen-coated 35-mm glass dishes (Asahi Techno Glass). After 24 h from seeding, the cells were washed once with PBS and fixed with 4% paraformaldehyde for 10 min. The cells were permeabilized with 100% methanol for 10 min and then immunostained with anti-Higd1a polyclonal antibody and anti-Cox4 monoclonal antibody. For secondary reactions, Alexa 488- or 568-labeled secondary antibodies (Invitrogen) were used.

The cells infected with adenovirus encoding carboxyl terminus Flag-tagged Higd1a (adHig), were treated with 50 nM of Mito-Tracker Red for 30 min, washed once with prewarmed PBS, and fixed using the same method described as above. For lebeling, anti-Flag M2 monoclonal antibody (Sigma-Aldrich) was used. Fluorescence images were recorded with an Olympus FV1000D confocal microscope using a PL APO 60×, 1.35 N.A. oil immersion objective lens (Olympus).

Pull-Down Assay. Cytochrome *c* oxidase from bovine heart was purified by the method reported previously (3–5). Recombinant MBP-Higd1a (5 μg) and highly purified cytochrome *c* oxidase (hpCcO) (20 μg) were incubated at 25 °C for 30 min in the presence of 0.2% *n*-decyl-β-D-maltoside (DM), and amylose resin was added at 4 °C for 1 h. After washing, bound proteins were eluted by SDS/PAGE sample buffer.

Blue Native PAGE. A total of 10 μg of mitochondrial pellets, as measured by using the Bradford method, from cardiomyocytes was solubilized, containing 2% (wt/vol) digitonin. Solubilized samples were incubated on ice for 10 min and centrifuged for 30 min at $100{,}000 \times g$ at 4 °C. Supernatants were added to Coomassie G-250 and resolved on a 4–16% Native PAGE Bis-Tris gel (Invitrogen). Initially run for 30 min with a constant voltage of 150 V using a cathode buffer (pH 7.0, 50 mM tricine, 7.5 mM imidazole, and 0.02% Coomassie G-250) and anode buffer (pH 7.0, 7.5 mM imidazole). Next, the cathode buffer was exchanged into the light cathode buffer (pH 7.0, 50 mM tricine, 7.5 mM imidazole, 0.002% Coomassie G-250) and run for another 75 min with a constant voltage of 150 V. After electrophoresis, proteins were transferred to PVDF membrane (0.45 μm, Millipore) using Mini Trans-Blot Cell Assembly (BIO-RAD, pH 8.3, 25 mM tricine, 192 mM glycine) with a constant voltage of 30 V.

Recombinant MBP-Higd1a and hpCcO were incubated at 25 °C for 30 min in the presence of 0.2% DM. The mixed solution was resolved by the same electrophoresis method and transferred to PVDF membrane by semidry method (pH 8.3, 25 mM tricine, 192 mM glycine, 20% (vol/vol) methanol, 0.04% SDS) for 60 min with a constant voltage of 15 V. Then, membranes were washed with 8% (vol/vol) acetic acid followed by deionized-distilled water. Each antibody was conjugated and detected with a CCD camera-based detection system (ImageQuant LAS-4000, GE Healthcare).

Measurement of Intact Cellular Respiration. Oxygen consumption rates were measured by XF96 Extracellular Flux Analyzer (Seahorse Bioscience) in unbuffered DMEM containing 25 mM glucose, 2 mM-L-glutamine, and 1 mM sodium pyruvate under basal conditions and in response to 1 μM oligomycin A, 0.5 μM fluorocarbonyl cyanide phenylhydrazone (FCCP) and 100 nM rotenone + 100 nM antimycin A (Sigma). For measurement, 6×10^4 cardiomyocytes were treated with each adenovirus (adLacZ or adHigd1a or shLacZ or shHigd1a).

Measurement of ATP Synthesis in Permeabilized Cardiomyocytes. Speed of ATP synthesis in cardiomyocytes (1.2×10^4 cells per well for shRNA-treated groups and 7.5×10^3 cells per well for adLacZ or adHigd1a-treated groups) permeabilized with 2% (wt/vol) digitonin was measured as described previously (6). In brief, after addition of assay buffer, the luminescence (produced ATP) was measured every minute for 15 min using ATP bioluminescence assay kit CLS II (Roche). Every time point of data was divided by a value of ATP production at 10 min in shLacZ or adLacZ groups. ATP production at 10 min in shLZ or adLZ was regarded as 1.0.

Cell Viability. A total of 5×10^5 cells of cardiomyocytes were transfected with either shHigd1a (shHig) or shLacZ (shLZ), cultured for 60 h, and then subjected to hypoxic conditions (1% oxygen) for another 24 h. After hypoxia, the cells were stained with 2 μg/mL propidium iodide (Sigma) and 2 μg/mL Hoechst 33342 (Dojin Chemical) at 37 °C for 30 min. The cells were analyzed using IN Cell Analyzer 6000 (GE Healthcare).

Structure Modeling. A docking model of the CcO and Higd1a was constructed as follows: The initial docking model was created in COOT (7) using the coordinates for the COX (Protein Data Bank, PDB: 3ABM, removal of TG1 and TG3) and the HIGD1A (PDB: 2LOM, model 6 of 20 structures) and then refined by energy minimization without any structure factor terms by the Crystallography and NMR system (8, 9).

Statistical Analyses. The comparison between two groups was made by *t* test (two tailed). For MASC assay, comparison was made by repeated two-way ANOVA. A value of $P < 0.05$ was considered statistically signifcant. Data represent mean ± SEM.

1. Kioka H, et al. (2014) Evaluation of intramitochondrial ATP levels identifies G0/G1 switch gene 2 as a positive regulator of oxidative phosphorylation. *Proc Natl Acad Sci USA* 111(1):273–278.
2. Klement P, Nijtmans LG, Van den Bogert C, Houstěk J (1995) Analysis of oxidative phosphorylation complexes in cultured human fibroblasts and amniocytes by blue-native-electrophoresis using mitoplasts isolated with the help of digitonin. *Anal Biochem* 231(1):218–224.
3. Tsukihara T, et al. (1995) Structures of metal sites of oxidized bovine heart cytochrome c oxidase at 2.8 A. *Science* 269(5227):1069–1074.
4. Shinzawa-Itoh K, et al. (1995) Effects of ethyleneglycol chain length of dodecyl polyethyleneglycol monoether on the crystallization of bovine heart cytochrome c oxidase. *J Mol Biol* 246(5):572–575.
5. Yoshikawa S, Choc MG, O'Toole MC, Caughey WS (1977) An infrared study of CO binding to heart cytochrome c oxidase and hemoglobin A. Implications re O2 reactions. *J Biol Chem* 252(15):5498–5508.
6. Fujikawa M, Yoshida M (2010) A sensitive, simple assay of mitochondrial ATP synthesis of cultured mammalian cells suitable for high-throughput analysis. *Biochem Biophys Res Commun* 401(4):538–543.
7. Emsley P, Lohkamp B, Scott WG, Cowtan K (2010) Features and development of Coot. *Acta Crystallogr D Biol Crystallogr* 66(Pt 4):486–501.
8. Brunger AT (2007) Version 1.2 of the Crystallography and NMR system. *Nat Protoc* 2(11):2728–2733.
9. Brünger AT, et al. (1998) Crystallography & NMR system: A new software suite for macromolecular structure determination. *Acta Crystallogr D Biol Crystallogr* 54(Pt 5): 905–921.
10. Acín-Pérez R, Fernández-Silva P, Peleato ML, Pérez-Martos A, Enriquez JA (2008) Respiratory active mitochondrial supercomplexes. *Mol Cell* 32(4):529–539.

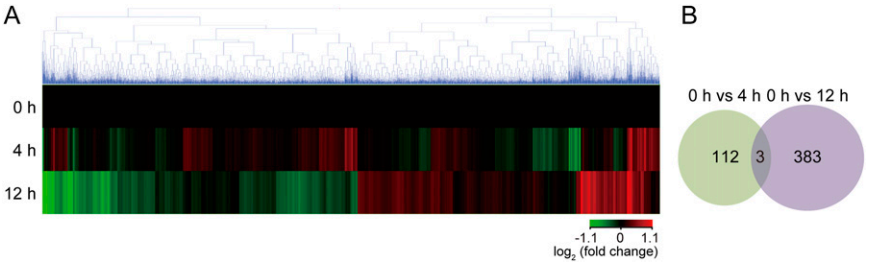

Fig. S1. Three genes were identified by microarray analysis using hypoxia-treated cardiomyocytes. (*A*) Hierarchical clustering image representing 2,598 genes exhibited significantly ($P < 0.05$; ANOVA) different expression levels at each of three time points (0, 4, and 12 h). (*B*) The Venn diagrams represented the overlap of genes that were up-regulated (>2.0-fold change up-regulated) at 4 h and genes that down-regulated (<1.2-fold change) by 12 h compared with 0 h, respectively.

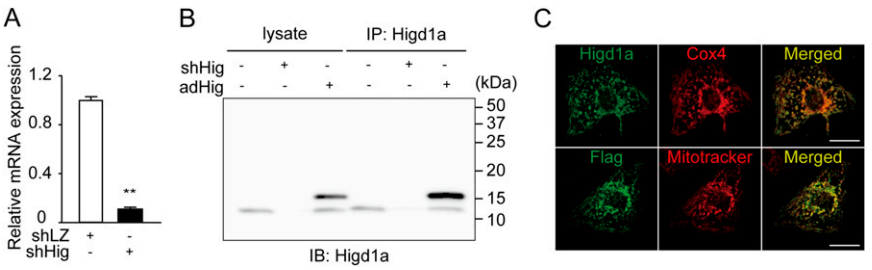

Fig. S2. Validation of our raised antibody against Higd1a. (*A*) Rat cardiomyocytes transfected with either shLacZ (shLZ) or shHigd1a (shHig) were analyzed by quantitative RT-PCR. *Higd1a* mRNA level was normalized by *Actb*. Data represent means ± SEMs ($n = 8$); $^{**}P < 0.01$, compared with control shLZ. (*B*) Validation of our established antibody for rat Higd1a. Immunoprecipitation was followed by immunoblot analysis of cardiomyocytes treated with shHig or adenovirus encoding carboxyl terminus Flag-tagged Higd1a (adHig). (*C*, *Upper*) Endogenous Higd1a was stained in cardiomyocytes with anti-Higd1a (green) and anti-Cox4 (red). (*Lower*) Cardiomyocytes transfected with adHig were stained with anti-Flag (green) and MitoTracker (red). The established antibody specifically recognizes neonatal rat Higd1a, which cannot be detected by commercially available Higd1a antibody (Scale bars, 20 μm.)

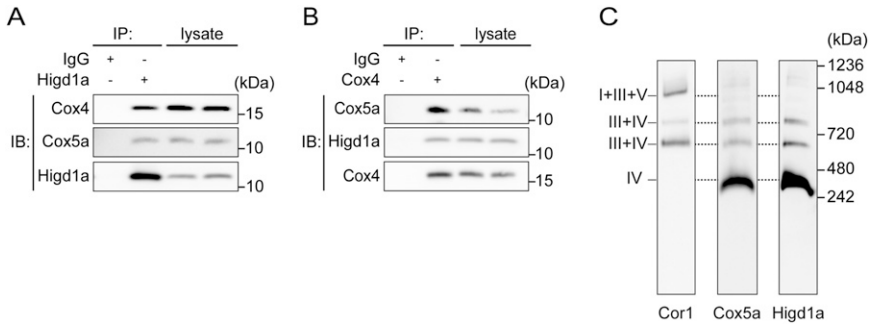

Fig. S3. Higd1a associated with CcO in rat cardiomyocytes. (*A*) Mitochondrial fractions isolated from rat cardiomyocytes were lysed and immunocaptured using an anti-Higd1a antibody and then immunoblotted with anti-Cox4 or anti-Cox5a antibodies to detect CcO subunits. (*B*) Reciprocal coimmunoprecipitation with an anti-Cox4, one of the subunits of CcO. (C) Mitochondrial fraction from rat cardiomyocytes was solubilized in 2% (wt/vol) digitonin and resolved by BN-PAGE, followed by immunoblotting with anti-Cox5a to detect complex IV or anti-Cor1 to detect complex III or anti-Higd1a. Higd1a integrated into the CcO, as it behaved similar to Cox5a, not to Cor1.

Fig. S4. Alignment of human Higd1a and bovine Higd1a with ClustalW (v 2.1). Black boxes, identical residues in both species; gray boxes, similar amino acids. Sequences of Higd1a are almost matched between human and bovine.

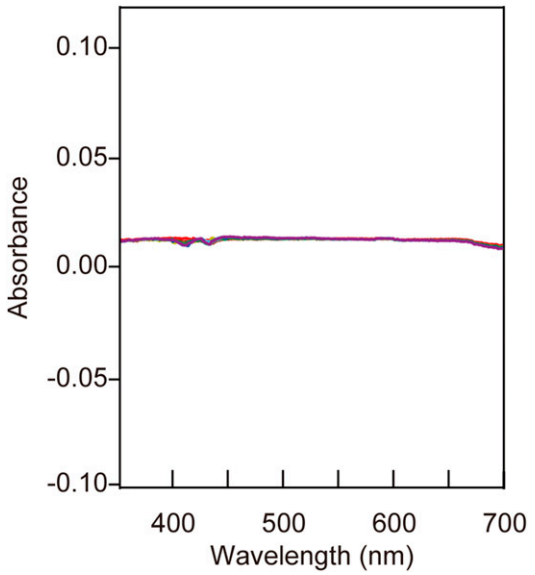

Fig. S5. Supporting data for Fig. 2. Optical absorption intensity changes of oxidized hpCcO spectra are plotted at 1 min (red), 5 min (brown), 10 min (dark yellow), 15 min (green), 20 min (light blue), 25 min (blue), and 30 min (purple) after adding MBP.

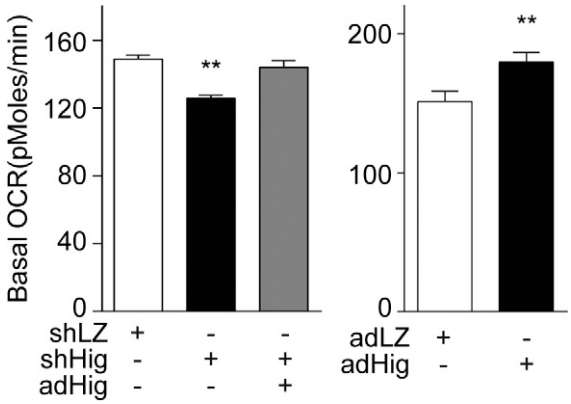

Fig. S6. Supporting data for Fig. 3. Basal oxygen consumption of rat cardiomyocytes transfected with either shLZ for control, shHig, or both shHig and adHig (n = 20 for each group).

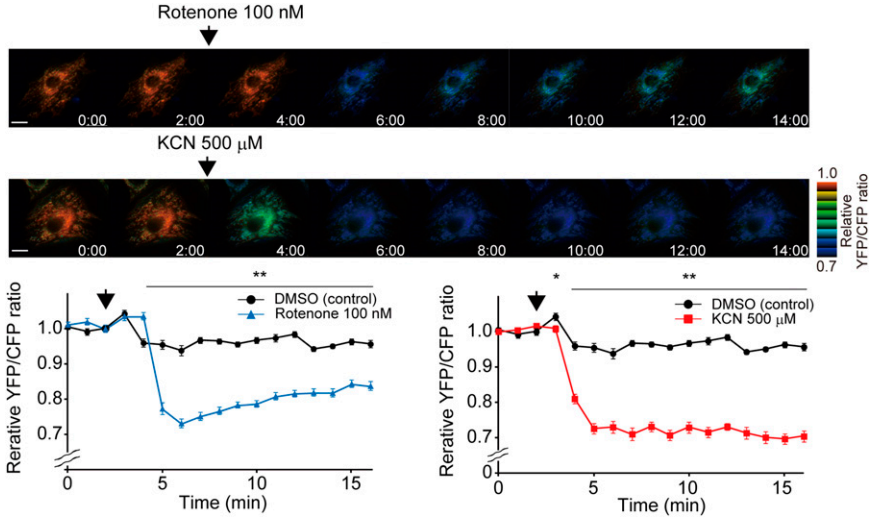

Fig. S7. Mit-ATeam assay reflects the function of complex I or IV. Mit-ATeam assay in rat cardiomyocytes is highly sensitive to assess the effect of inhibitors of rotenone (inhibitor of complex I) or KCN (inhibitor of complex IV) on mitochondrial oxidative phosphorylation. *Lower* line graphs represent YFP/CFP emission ratio plots of Mit-ATeam in rat cardiomyocytes. Rotenone (100 nM) or KCN (500 μM) was added at 2 min (arrowhead; n = 8), respectively. All measurements were normalized to the YFP/CFP emission ratio at 0 min. Data represent means ± SEMs. (Scale bars, 20 μm.)

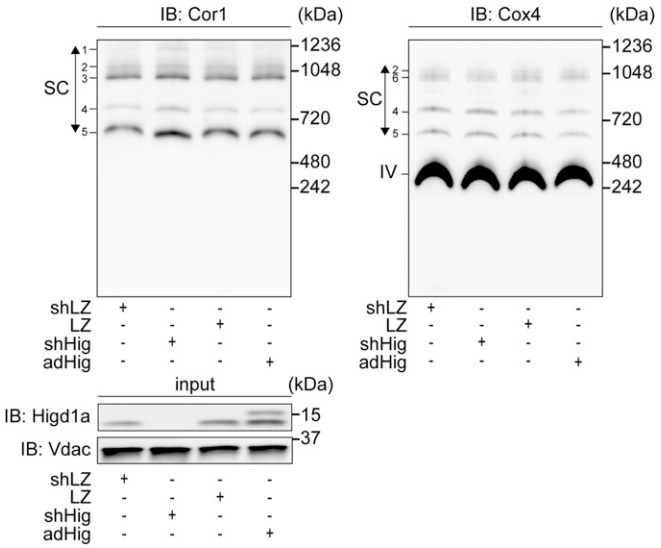

Fig. S8. Higd1a does not affect respiratory supercomplex formation. Mitochondrial fraction from rat cardiomyocytes transfected with corresponding viruses was solubilized in 2% (wt/vol) digitonin and 8 μg of each fraction was subjected to BN-PAGE, followed by immunoblotting with anti-Cox4 to detect complex IV or anti-Cor1 to detect complex III. The numbers, which are located on the *Left* side of the two *Upper* Western blots, represent respiratory supercomplex, specifically: 1 (I + III + V); 2 (I + II + III + IV); 3 (I + III + V); 4 (III + IV); 5 (III + IV); and 6 (I + III + IV) (10). *Lower* blot represents SDS/PAGE of inputs. Loading control, blotted with anti-VDAC antibody.

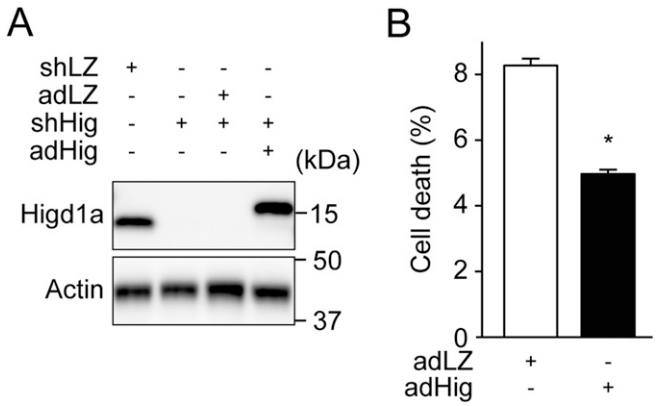

Fig. S9. Supporting data for Fig. 4*B*. (*A*) Immunoblotting of Higd1a treated with corresponding adenoviruses. (*B*) The cell viability was increased by exogenous adHig compared with adLZ under hypoxia for 14 h. Data represent means ± SEMs. $*P < 0.05$, $**P < 0.01$, compared with control (adLZ or shLZ).

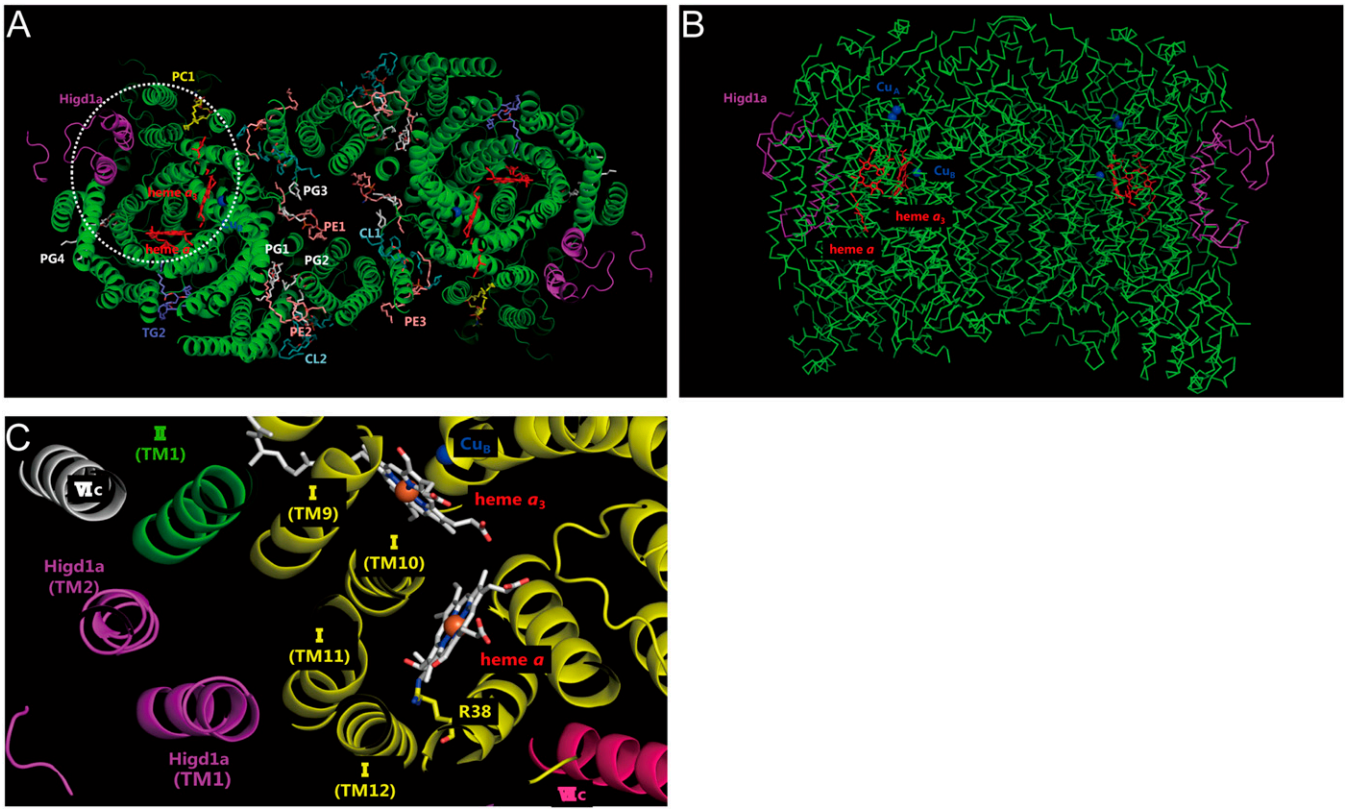

Fig. S10. Docking simulation between CcO (PDB accession code: 3ABM, removal of TG1 and TG3) (the Cα backbone trace: green) and Higd1a (PDB accession code: 2LOM, model 6 of 20 structures) (magenta). Higd1a integrated into the cleft of CcO, just outside of the active center. (*A*) Top view. (*B*) Side view. CL 1–2, cardiolipin (light blue); PC, phosphatidylcholine (yellow); PE 1–3, phosphatidylethanolamine (pink); PG 1–4, phosphatidylglycerol (white); and TG 2, triglyceride. (*C*) Enlarged image of docking simulation (dotted white circle in *A*). The TM1 of Higd1a (magenta) is near the TM11 and TM12 of subunit I (yellow) and it is likely that the binding of Higd1a affects the structure of R38 (yellow) and formyl group of heme *a*.